CONF-9[illegible]
ANL/CP--76359

DE92 016397

Invited Paper to be presented at the 7th Annual Congress of the Brazilian Microelectronics Society, Sao Paolo, Brazil, July 6-10, 1992

Ion Beams as a Means of Deposition and in-situ Characterization of Thin Films and Thin Film Layered Structures

A. R. Krauss[1], M. Rangaswamy[1], J. A. Schultz[2], H. Schmidt[3], Y. L. Liu[1,4], O. Auciello[5], T. Barr[4], Y. P. Lin[1,6], D. M. Gruen[1] and R. P. H. Chang[6]

[1]Argonne National Laboratory Materials Science and Chemistry Divisions, [2]Ionwerks Corporation, Houston, TX, [3]Schmidt Instruments Corporation, Houston, TX, [4]Materials Science Dept., University of Wisconsin-Milwaukee, Milwaukee WI, [5]MCNC Microelectronics Center of N. Carolina, [6]Northwestern University Department of Materials Science

A system for the sequential deposition of multi-component metal and metal oxide thin films and layered structures by ion beam deposition from multiple targets has been developed. By controlling the layer thickness, deposition rate, oxygen (or nitrogen) flow rate, and substrate temperature via a computer feedback system, the intrinsically layered film structure produced by this system may either be retained or homogenized to a uniform multi-component film. The method has been successfully used to produce complex multicomponent and multilayered thin films containing ferro-electric, electro-optic, magnetic and high temperature superconducting materials, and appears to be applicable to the fabrication of hybrid devices incorporating several different categories of materials. The characterization of the relevant processes during thin film growth in such a system however, turns out to be beyond the capabilities of most techniques of in-situ characterization. However, low energy (5-15 keV) pulsed ion beam surface-analytical techniques possess the ability to provide a remarkably wide range of information directly relevant to the growth of multi-component semiconductor, metal and metal oxide thin films and layered structures. The information available with these methods includes the surface composition, atomic structure of the first few monolayers, lattice defect density, trace element analysis and phonon characteristics. Much of this data may be obtained on samples which are at ambient gas pressures up to one torr, i.e. 6-8 orders of magnitude higher than any other analysis technique which provides a comparable degree of surface specificity. This capability makes pulsed ion beam analysis ideal for real-time, in-situ characterization of thin film growth processes. We discuss here some of the materials properties which may be measured by Direct Recoil Spectroscopy, (DRS), Ion Scattering Spectroscopy (ISS) and Mass Spectroscopy of Recoiled Ions (MSRI), and describe a physical implementation of the pulsed ion beam analysis technique which requires very low beam dose, provides real-time data acquisition, does not interfere physically with thin film deposition equipment, is compatible with high ambient pressure operation, and is therefore suitable as a real-time probe of thin film deposition.

Work supported in part by the U. S. Department of Energy, Office of Basic Energy Sciences under contract W-31-109-ENG-38 and by the State of Illinois Dept. of Commerce and Community Affairs

Ion Beams as a Means of Deposition and in-situ Characterization of Thin Films and Thin Film Layered Structures

Introduction

Ion beams may be used to deposit thin films and layered thin film structures, modify films deposited by other methods, and characterize the surfaces of films and bulk materials. Although some of the same phenomena occur for plasma processing, this review is largely limited to beam sources. With ion beams, it is possible to provide better control of the flux and kinetic energy, ion species, charge state and angle of incidence, as well as to provide lower contamination by chamber wall materials than is possible with plasma methods. In general, ion beam sources operate at lower pressures than plasma devices, and therefore the mean free paths of the incident primary ions, sputtered target materials and backscattered primary ions are relatively long, and there is little thermalization . Consequently, the kinetic energies associated with both the primary beam and sputtered atoms are relatively high, resulting in phenomena which may either promote desirable film properties such as film-substrate adhesion and surface smoothness, or cause film damage and alter film stoichiometry, depending on the manner in which deposition and post-deposition processing are carried out.

Thin film deposition systems which produce complicated multi-component films and layered structures for advanced device applications require some means of in-situ monitoring of film growth. As an example of such a deposition system, we have been using a single ion beam, multi-target (SBMT) sequential deposition method [Krauss 1990, Kingon 1991] for the production of $YBa_2Cu_3O_{7-x}$ thin films and layered structures. In the SBMT method, very thin layers of material are deposited sequentially using elemental, alloy or simple oxide targets. Depending on the layer thickness and the thermal treatment, it is possible to either retain the layered structure or produce a uniform multicomponent film. One of the driving forces for developing this method is its applicability to integrated fabrication and processing of hybrid layered structure devices incorporating materials representing semiconducting, ferroelectric, optoelectronic, magnetic and high temperature superconducting technologies. We have made successful films of representative materials from all of these categories, but the largest effort has been focused on the $YBa_2Cu_3O_{7-x}$ high temperature superconducting (HTSC) materials.

Regardless of the deposition method, the best $YBa_2Cu_3O_{7-x}$ thin films have critical current densities approximately 100x higher than bulk polycrystalline material. A connection has been made [Hawley 1991] between the high critical current density observed in some HTSC thin films and a high density of screw dislocations believed to be associated with island growth during the early stages of film nucleation. The ability to characterize the early stages of film formation would provide a means of unambiguously identifying the growth processes which lead to high J_c values, and help to assure the attainment of those growth conditions.

The number of analytical techniques however, which are suitable for *in-situ* characterization of surface processes during thin film growth is very limited. Techniques such as x-ray diffraction and x-ray fluorescence spectroscopy can be used for *in situ* characterization of the overall properties of a film, but except for grazing incidence geometries, they sample the material to a depth on the order of 0.5 to 1 μm. In order to characterize the processes occurring at the surface of a growing film, it is necessary to probe the first few atomic layers, and in principle to identify the uppermost monolayer where the growth occurs.

All surface analysis schemes involve directing ions, electrons, or photons onto the sample, and detecting the ejected ions, electrons, or photons resulting from a number of different physical processes within the solid. For example, X-ray Photoelectron Spectroscopy (XPS) involves the impact of an incident x-ray beam on the analyzed material to create photoelectrons. The kinetic energy of these photoelectrons is uniquely related to the electron energy levels of the atoms within the solid and can therefore be used to identify the atoms. The surface sensitivity of XPS is due to the fact that only photoelectrons generated in a shallow layer near the surface can escape to the vacuum to be detected. For electrons with a kinetic energy $\leq$ 1 keV, the depth of analysis varies from approximately 5 to 40 Å. However, if there is an ambient gas pressure associated with the deposition process, the short electron mean free path becomes a disadvantage since the electron must travel distances on the order of 0.5 meters through an energy analyzer before it reaches the detector. Techniques such as Auger Electron Spectroscopy (AES), Ultraviolet Photoelectron Spectroscopy (UPS), Low Energy Electron Diffraction (LEED), and XPS typically require high to ultra-high vacuum ($<10^{-8}$ torr) in the region surrounding the sample.

There is an additional practical constraint on most surface analytical methods in regard to in-situ monitoring of thin film deposition in that the analysis equipment must not intrude in the area occupied by the deposition equipment. In order to obtain relatively high data acquisition rates, most surface analytical equipment requires the positioning of large instrumentation very close to the sample surface. There are several techniques which utilize relatively collimated beams and therefore do not interfere with the deposition process. Reflection High Energy Electron Diffraction (RHEED) utilizes elastically scattered electrons with a kinetic energy in the range of 20 keV. This energy is high enough to provide a reasonably long electron mean free path. RHEED is therefore widely used in molecular beam epitaxy (MBE) systems where the ambient pressure during deposition is relatively low. RHEED provides a measure of the lattice spacing in the direction normal to the substrate, but provides no chemical identification and no information on short-range phenomena such as pinhole formation.

As an example of a surface analytical method which is suitable to in-situ analysis of thin film growth for multi-component metal, metal oxide, and nitride films, we will describe a pulsed ion beam surface analysis system which is under development as an in-situ, real-time monitor of film properties.

Ion Beam Deposition of Thin Films

There are a number of advantages relating to ion beam deposition of thin films. Compared with plasma sputtering systems, it is much easier to reduce or eliminate interactions between the energetic ions and deposition chamber structures, thereby producing films with low impurity content. Compared with thermal or chemical vapor deposition (CVD) methods, the relatively high kinetic energies associated with both the sputtered target atoms and the backscattered primary ions incident on the substrate can result in improved adhesion, and denser films. [Weissmantel 1979,1982,Harper et. al. 1984] In addition, Weissmantel [Weissmantel 1981] has shown that conditions corresponding to high pressures and temperatures can be produced in the collision cascade, resulting in the production of materials which are not thermodynamically stable at the ambient pressure and substrate temperature conditions under which the deposition occurs. Several examples of kinetic energy-related effects are presented here:

Metals and Semiconductors

In order to provide greater control of the degree to which kinetic energy is deposited in the growing film, it is a common practice to use one ion source to produce the film by sputtering the target, in the vicinity of the substrate, and a second ion source directed at the film. This second

source can be independently adjusted without affecting the deposition flux. For metal films, the resulting grain size depends on the primary ion kinetic energy deposited per film atom. In general, the effect of ion bombardment is to increase the grain size [Linnros 1984, 1985, Williams 1985, Atwater 1986, Wang 1986, Liu 1987a, 1987 b]. Results for Au, Si and Ge thin films have been adequately described by a model [Atwater et. al.1988] based on momentum transfer between the energetic ion and beam-generated Frenkel defects, with consequent motion of the grain boundaries. However, Li et. al. [Li 1989] observed significant differences in grain growth for ion bombarded Pt and Au films which did not fit the Frenkel defect model which predicts similar grain growth since Pt and Au have similar masses. For these materials, a thermal spike model [Alexander 1991] provided a better fit to the experimental results. For Ar^+ ion bombardment of Ag, it has been found [Huang 1985] that the grain size decreases with increasing kinetic energy for deposited energies up to 40 eV per silver atom, after which grain size remains approximately constant. In general, Ion bombardment during the initial stages of deposition can strongly alter the surface defect density, thereby altering both the nucleation process and the density of defects in the film. Films deposited with concurrent ion beam bombardment are typically less porous than thermally deposited films, and are therefore denser and more resistant to atmospheric attack. For optically transmitting materials, such films have a higher index of refraction than films deposited by purely thermal means. For metals, the presence of defects enhances the film hardness.

In general, metal films deposited at room temperature are randomly oriented, forming well-oriented crystals only after annealing at elevated temperatures. However, it has been demonstrated [Ziemann 1983] that fcc metal films grown at room temperature on amorphous substrates have a large fraction of their (111) lattice planes parallel to the substrate if they are subjected to Ar^+ ion bombardment during growth. Similarly, it has been found [Thomas 1982, Zalm 1982] that the minimum temperature required for epitaxial growth can be significantly reduced through ion bombardment concurrent with film growth.

Stresses which occur at the interface between the film and substrate can lead to degradation of device performance and, in extreme cases, to peeling of the film from the substrate. The use of ion beam impact can modify film stress in several ways: "Ion beam stitching" caused by recoil implantation of some of the film atoms into the substrate results in a graded interface which can distribute the stress over a broader area, thereby lessening the likelihood of film-substrate fracture. Implantation of beam ions results in an enlargement of the average lattice constant, thereby converting tensile stress into compressive stress. The high effective temperature in the region of the collision cascade also leads to an annealing effect, which relieves stress regardless of whether it is tensile or compressive. For growing films, surface atom migration is enhanced, resulting in enhanced chemical activity and the formation of phases otherwise associated with high temperature growth processes [Takagi 1984].

It should be noted that beam-related effects are not always beneficial. For example, Pt/Co multilayer thin films have attractive properties for magneto-optical recording. Ion beam deposition is an effective means of producing such multilayers, but it has been found that enhanced interfacial mixing and structural damage associated with reflection of the Ar^+ primary beam back to the film results in reduced magnetic coercivity [den Broeder, 1987]. Ar is reflected very efficiently from high mass atoms such as Pt, but heavier ions such as Kr and Xe are not [Ameen 1990, Krauss 1992, Eckstein 1991]. It has been demonstrated that the use of Kr^+ or Xe^+ as the ion species results in films with sharper Pt-Co interfaces which exhibit larger magnetic coercivity than films deposited using an Ar^+ beam [Carcia 1990].

Diamond Thin Films

Diamond thin films are of extreme importance to a number of technological applications. Because of its high dielectric strength ($2x10^7$ volts/cm *vs* $5x10^5$ volts/cm for SiO_2) and thermal conductivity (20 W/cm/K), diamond used either as an insulating gate for conventional Si-based devices, or directly as a high temperature semiconductor, should be able to significantly increase the voltage, temperature, power and frequency specifications of electronic devices. The extreme hardness of diamond makes it suitable as a tribological coating to enhance the life of cutting tools. Additionally, the large band gap (5.5 eV) makes diamond suitable for wide wavelength range optical windows, X-ray windows, lasers & LEDs. There are however, a number of problems associated with current diamond thin film deposition technology: In order to take advantage of the high dielectric strength of diamond to make high voltage, high frequency field effect transistors, it is necessary to produce very thin films of uniform thickness. High temperature Chemical Vapor Deposition (CVD) is commonly used to grow diamond and diamond-like films, typically using a mixture of CH_4 and H_2. There is some controversy concerning the exact function of the hydrogen in CVD deposition, but it appears that essentially any process which generates atomic hydrogen in the presence of methane and a heated substrate is able to produce diamond or diamond-like films. Part of the function of the atomic hydrogen seems to be to preferentially etch the graphitic phase, thereby enhancing the relative growth of the diamond phase. It has also been noted that adsorbed hydrogen stabilizes the sp^3 electronic bonding which is characteristic of the diamond phase.

The CVD process is capable of rapidly growing large area films, but requires a substrate temperature in the range 900-1000 °C, making it unsuitable for silicon-based semiconducting device technology. Additionally, it is very difficult to obtain high nucleation density on most substrates with the CVD process, and the usual method of promoting diamond growth is to abrade the surface with diamond powder, leaving behind a residue of very small diamond crystallites. This process is not only not compatible with the requirements of semiconductor device processing, but leads to the formation of widely dispersed crystallites which form a continuous film only when the film thickness is great enough for the crystallites to merge. Typically, it is difficult to grow continuous diamond films less than 5 μm thick.

For tribological applications, the non-uniform growth also causes performance limitations. Although gains in tool life of 10^2-10^3 have been obtained, compared with uncoated tools, the typical failure mode of diamond-coated tools consists of diamond crystallites fracturing at the interface, rather than wear of the grain faces. For optical applications, free-standing diamond films have been made. In general, such films have a high density of imperfections which increases the optical density. Additionally, such films are usually very rough, resulting in diffuse, rather than specular light scattering.

For metals and semiconductors, we have noted that the problems of nucleation, film adhesion, stress relief, surface roughness, lack of crystallinity and high required processing temperatures are all amenable to improvement by ion beam processing. Calculations by Weissmantel [Weissmantel 1981] suggest that the high transient temperatures and pressures associated with the collision cascade should stabilize the sp^3 bonded structure of diamond. It has also been noted [Miyazawa 1984, Angus 1986] that for sufficiently energetic carbon ions, sputtering will preferentially remove the graphitic phase which has a lower surface binding energy and therefore a higher sputtering yield than the diamond phase. The Monte Carlo computer code TRIM has been used [Moller 1991] to calculate the relative growth rates of the graphitic and diamond-like phases during ion beam sputtering.

Experimentally, diamond-like films were first grown by a method of direct deposition of carbon ions generated by sputtering of a sacrificial carbon cathode, or through the use of a volatile

carbon-bearing gas [Holland 1978, Berg 1979, Tschersich 1989]. The carbon sputtering method is able to produce small crystallites of true diamond, although the bulk of the film area appears to be covered with an amorphous carbon coating containing little or no hydrogen. However, the very low deposition rates, small deposition area (~0.1 cm^2) and non-uniform film thickness produced by these sources made the resulting films very difficult to characterize. It has been reported [Kasi 1987, 1988, Kulik 1992] that direct carbon ion deposition at kinetic energies in the range 30-175 eV produces hard, amorphous carbon films with diamond-like properties on room temperature substrates. The electronic binding for these films has been measured as 58% sp^3. The recent discovery [Meilunas 1991] that a layer approximately 1000 Å thick of the C_{70} fullerene molecule, after being subjected to an ion beam bombardment, provides a vacuum compatible means of nucleating diamond film growth with much higher density than that provided by diamond abrasion of the surface may result in a renewed investigation of ion-assisted growth processes for the deposition of diamond and diamond-like thin films.

High Temperature Superconductors

Most of the copper oxide high temperature superconductors contain high mass components, such as Ba in $YBa_2Cu_3O_{7-x}$ and Bi in the Bi-Sr-Ca-Cu-O series of superconducting materials. These high mass components have low surface binding energies and therefore a comparatively high sputtering yield. For relatively light primary ions such as argon, there is a high degree of backscattering from these target materials, and consequently significant secondary sputtering of the film. For dc magnetron sputter-deposition of $YBa_2Cu_3O_{7-x}$, contradictory claims have been made concerning the effect of energetic particle impact on the film during growth. Muroi et. al. [Muroi 1992] found that when the sputtered target atoms were thermalized by gas phase collisions before reaching the substrate, the substrate temperature had to be at least 650 °C in order for the orthorhombic superconducting $YBa_2Cu_3O_{7-x}$ phase to be formed. If on the other hand, gas phase collisions were minimized, allowing the sputtered atoms to retain their initially high kinetic energies, it was possible to form the superconducting phase at temperatures as low as 500 °C. Selinder at. al. [1991] have found that for dc magnetron sputtering from stoichiometric $YBa_2Cu_3O_{7-x}$ targets, the films are stoichiometric only if they are deposited in a relatively high pressure (>9 Pa) of Ar. If the argon pressure is less than 6 Pa, the films are copper-deficient. For an Ar pressure of 2 Pa, films deposited at 200 °C are copper deficient by approximately 20%. However, at the more customary substrate temperature of 600 °C, the Cu in the film is less than 20% of the formula value. The failure to reproduce the target stoichiometry at lower pressures is attributed to selective resputtering by energetic oxygen bombardment during film growth. For high oxygen pressures, it has even been found [Rossnagel 1988] that negative deposition (i.e. net etching) of the film occurs.

We have conducted several studies of $YBa_2Cu_3O_{7-x}$ thin film deposition using Ar, Kr and Xe ion beams. One set of films was deposited as a sequentially layered structure using Y, BaCu alloy and pure Cu targets as shown in Fig. 1, with a jet of molecular oxygen incident on the substrate which was held at a temperature ranging from room temperature to 700 °C. Sequential ion beam deposition from multiple targets constitutes an attractive approach to the deposition of multi-component films since it is possible to deposit a variety of materials by a single process which is therefore applicable to the fabrication of devices incorporating a number of different types of materials for superconducting, semiconducting, magnetic, ferroelectric and electrooptic applications [Ameen 1989, Krauss 1990].

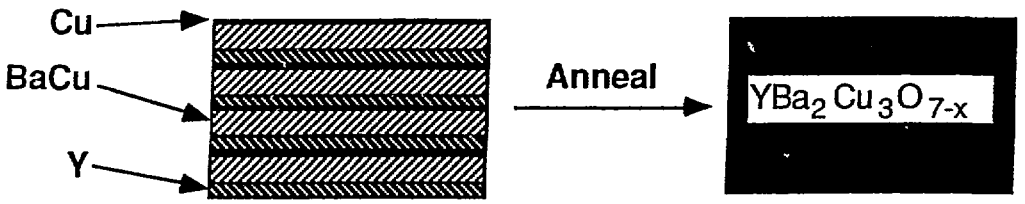

Fig. 1. Layered thin film structure produced by depositing $9x10^{15}$ atoms/cm^2 of Y, $2x10^{16}$ atoms/cm^2 of BaCu from a BaCu alloy target, and $2x10^{15}$ atoms/cm^2 of Cu. The sequence is repeated until the desired film thickness is reached. Subsequent high temperature annealing produces a uniform composition.

The thicknesses of the layers shown in Fig. 1 were set to $9x10^{15}$ atoms/cm^2 of Y, $2x10^{16}$ atoms/cm^2 for the BaCu alloy and $2x10^{15}$ atoms/cm^2 for the pure Cu target. The amount of each component actually deposited was controlled by feedback to the deposition control computer using a quartz crystal thin film monitor as the feedback element. For temperatures below 550 °C, the amount of each component retained in the film depends on the ion beam mass but not on the substrate temperature; films deposited using a 4 keV Ar^+ beam were deficient in both Ba and Cu compared with films deposited with a 4 keV Xe^+ beam, while Kr^+-deposited films were intermediate between Ar^+ and Xe^+. As the substrate temperature increases, the relative losses of Ba and Cu increase as a result of thermal desorption. For Kr^+ and Xe^+ beams with the substrate at 650 °C, the loss of Ba and Cu is dominated by thermal desorption and the loss rates are almost identical for the two beam gases. Ar^+ however still shows an enhanced loss of Ba and Cu as a result of secondary sputtering of the film by backscattered primary ions.

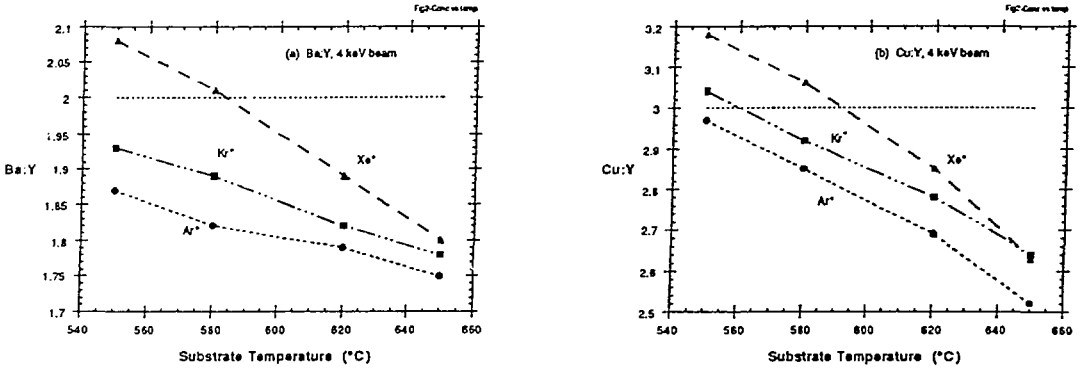

Fig. 2. HTSC Ba:Y (a) and Cu:Y (b) film stoichiometry as a function of substrate temperature for 4 keV ion beam deposition using three different ion species. The films were deposited according to the scheme depicted in Fig. 1 Nominal concentrations of Ba and Cu are shown by the horizontal dashed lines at 2.0 and 3.0 respectively.

Post-deposition annealing was used to mix the layers and to form the superconducting orthorhombic crystal structure. The annealing schedule consisted of heating from room temperature to 875 °C, holding the film at that temperature for 15 minutes in order to form the tetrahedral structure, and then reducing the temperature to 475 °C, where it is held for several hours in order to bring the lattice oxygen up to a value close to 7.0. By conducting the initial heating in an

atmosphere of pure Ar, some of the lattice oxygen is lost, resulting in the formation of BaCu and Cu sub-oxides which melt at temperatures <875 °C. Recrystallization from the melt forms a single phase, c-axis oriented $YBa_2Cu_3O_{7-x}$ thin film with a superconducting transition temperature 92.5-93 K and a transition width ~0.5 K as shown in Fig. 3. The film shown in Fig. 3a was produced using a 4 keV Xe^+ beam, but films of comparable quality can be produced with an Ar^+ ion beam, as seen in Fig. 3b. The c-axis lattice spacing as measured by x-ray diffraction was found to be 11.68 Å, in excellent agreement with the lattice parameter of single crystal $YBa_2Cu_3O_{7-x}$. It should be noted however, that unless these films exceed approximately 6000 Å in thickness before annealing, they become spatially inhomogeneous, exhibiting bare areas of unwetted substrate as shown in Fig. 4.

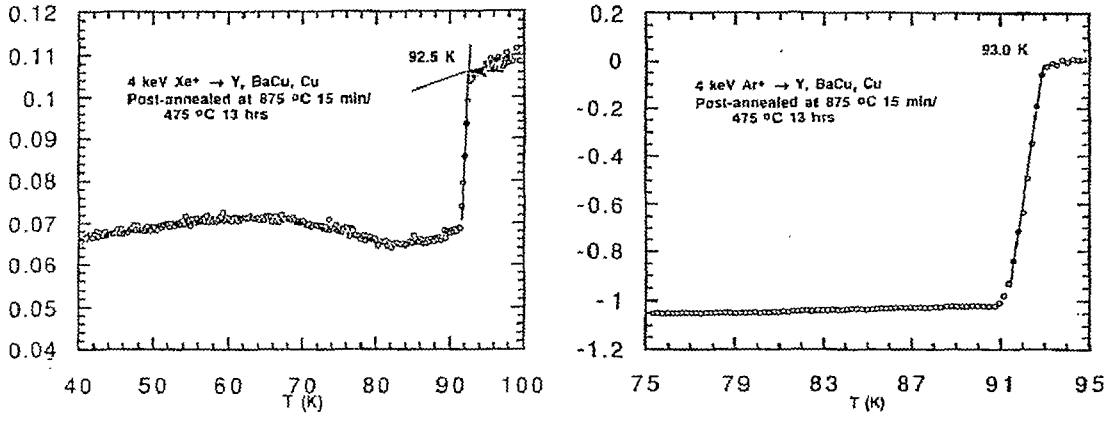

Fig. 3. Adiabatic magnetization measurement of two $YBa_2Cu_3O_{7-x}$ thin films which were deposited sequentially as indicated in Fig. 1 and then annealed. The ion beams were (a) 4 keV Xe^+, and (b) 4 keV Ar^+ . The superconducting transition occurs where the two slopes intersect.

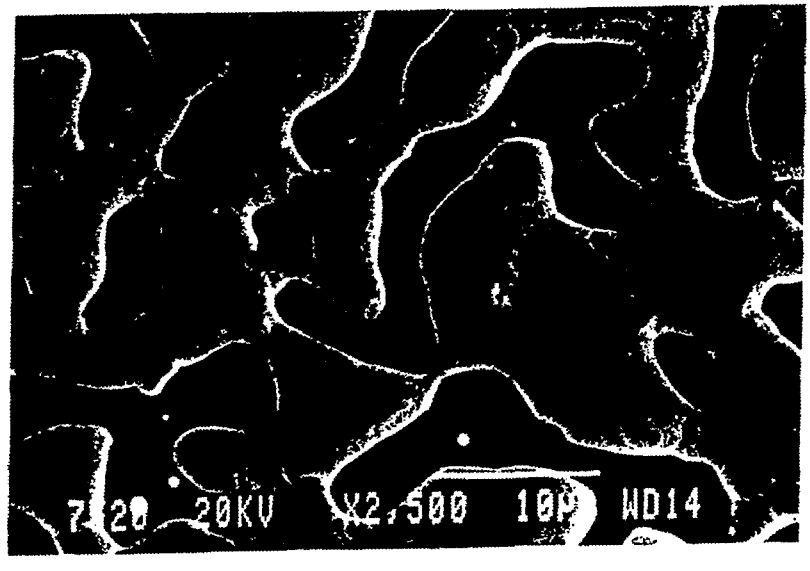

Fig. 4. Secondary electron micrograph of a $YBa_2Cu_3O_{7-x}$ thin film which was deposited sequentially as indicated in Fig. 1 and then heated in a pure Ar atmosphere prior to recrystallization and completion of the oxidation process.

By using atomic oxygen, ozone, or a locally high pressure of molecular oxygen and depositing an intimate mixture of components, it is possible to produce $YBa_2Cu_3O_{7-x}$ thin films which are superconducting in the as-deposited state. In order to take advantage of the possibilities for in-situ fabrication of complex multilayered devices inherent in the sequential ion beam deposition method, it is of course necessary to avoid post-deposition ex-situ, high temperature annealing steps. Because of the very short superconducting coherence length in the high temperature superconducting oxides (5-15 Å), device fabrication using these materials requires the formation of exceptionally smooth, extremely thin layers, free of pinholes. It has been demonstrated that ion beam deposition is capable of producing as-deposited superconducting thin films with a surface roughness of 6 Å [Lichtenwalner 1992].

Typically however, the superconducting transition temperature and the critical current density are lower for the as-deposited films than they are for the post-deposition annealed films. Ion beam-deposited films which are superconducting as-deposited usually exhibit an enlarged c-axis lattice spacing, suggesting the presence of either trapped gas or a high defect density [Kittl 1990a, 1990b, 1991]. As shown in Fig. 5 [Soble 1992], the transition temperature is a strong function of ion mass and energy. Eckstein & Biersack have shown that the primary ion reflection yield drops sharply if the mass of the ion beam is greater than that of the target atoms [Eckstein 1986]. We therefore anticipate that the lower transition temperatures observed for high primary ion mass and kinetic energy result from either lattice damage or gas implantation associated with primary ion backscattering. Using the TRIM computer code to model the flux, kinetic energy distribution, and angular distribution of both the sputtered target atoms and the scattered primary ions incident on the substrate, we have been able to calculate the trapped beam gas and kinetic energy which is deposited into pure Y, Ba and Cu films [Krauss 1992].

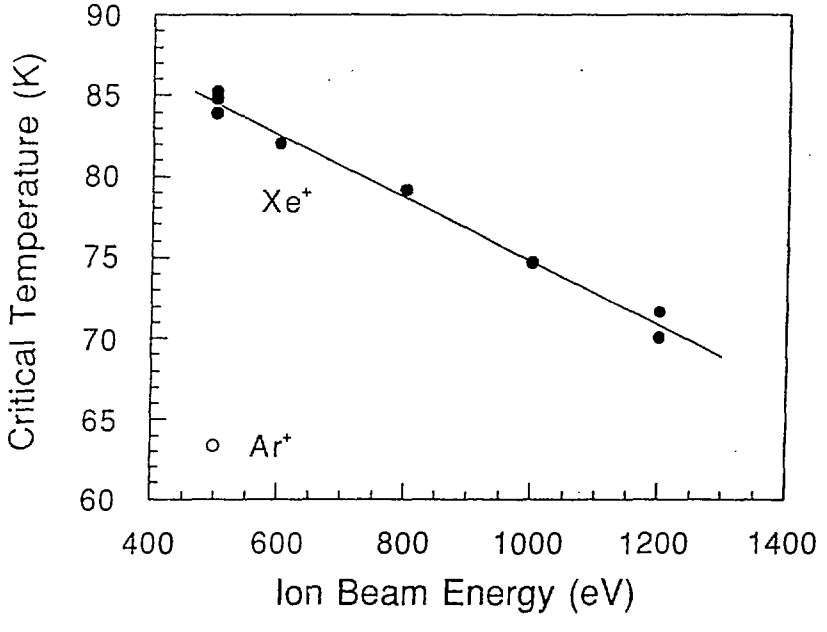

Fig. 5. Superconducting transition temperatures of as-deposited $YBa_2Cu_3O_{7-x}$ thin films as a function of ion beam mass and kinetic energy.

In general, it is found that the film damage increases with increasing primary ion energy, while the trapped gas decreases with increasing primary ion energy. Bombardment of the growing film by scattered Ar^+ ions results in the largest damage and trapped gas, while bombardment by Xe^+ results in the least. Regardless of the primary ion mass , 45° incidence of the primary beam on the target results in significantly more damage and gas implantation than normal incidence, in spite of the higher deposition rate associated with off-normal incidence. Finally, the low surface binding energy of Ba and high reflection coefficient, especially for relatively low mass primary ions such as Ar^+, makes Ba much more susceptible to beam damage and gas implantation than Cu or Y.

A comparison of Figs. 6a and 6b indicates that for a normally incident ion beam, the damage produced in the growing film by Ar^+ ions scattered from a Ba target is about an order of magnitude larger than the damage produced by Ar^+ ions scattered from a Cu target. For Kr^+ ions incident on Ba, the damage is approximately one order of magnitude lower than for Ar^+ incident on Ba, while the damage associated with Xe^+ incident on Ba is an additional factor of ten lower. For the Kr^+ and Xe^+ beams incident on a Cu target, the indicated damage/growth ratio is 3-4 orders of magnitude lower for the Ar^+ beam incident on Cu. The apparent equivalence between Kr^+ and Xe^+ is actually a result of the very low number of scattering events predicted by TRIM for these particle-target material combinations, and is to be taken as an upper limit for the actual damage/growth ratio.

The amount of gas trapped in the film decreases with increasing energy for all three primary ions scattered from Ba and for the Ar^+ ions reflected from Cu. However, for the latter target material, not a single scattering event in 10^4 particle histories was predicted for either Kr^+ or Xe^+, and it is concluded that for normal incidence virtually no Kr^+ or Xe^+ will be trapped in the film. Two relevant features of Fig. 6a should be pointed out; that is, the damage produced by scattered Xe^+ ions decreases noticeably when the energy of the primary beam impacting on the target is reduced from 1000 eV to 500 eV, while the amount of trapped gas increases. This indicates that damage produced in the growing film by the scattered ions, rather than trapped beam gas, may be the dominant degradation mechanism for the as-deposited superconducting films.

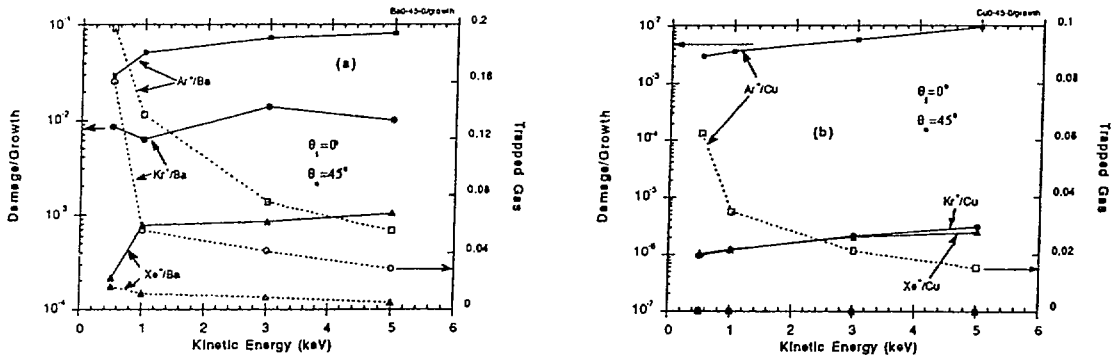

Figure 6. Normalized damage/growth and trapped gas curves, related to the synthesis of YBCO films by ion beam sputtering of elemental targets. The calculations are for Ar^+, Kr^+, and Xe^+ ions impacting on Ba (a) and Cu (b) at normal incidence, with the substrate at 45°, as a function of kinetic energy of the primary ion.

The calculations of lattice damage and the amount of trapped gas in the growing film for all ions impacting on Ba and Cu at 45° , with substrate placed at 45° relative to the target normal (θ_i = 45° and θ_o = 45°) are presented in Figs 7a and 7b, respectively. The general trends of all curves

presented in Figs. 7a and 7b as a function of the primary ion beam energy are similar to the case of normal incidence. However, there are four distinctive differences, namely: (a) the damage produced by Xe^+ ions scattered from Ba and Cu, for a 45° primary ion incidence, are about one and three orders of magnitude larger, respectively, than the damage produced for normal incidence (Figs. 6a and 6b); (b) the difference in the film damage for the three ion species is not as large as it is in the normal incidence case (Figs. 6a and 6b); (c) there is a noticeable difference in the damage produced by Kr^+ ions with respect to that produced by Xe^+ when scattered from Cu (Fig. 7b); (d) the amount of trapped gas is consistently higher than for normal incidence. Specifically, there is no target material, primary ion mass or kinetic energy for which no scattering events are observed.

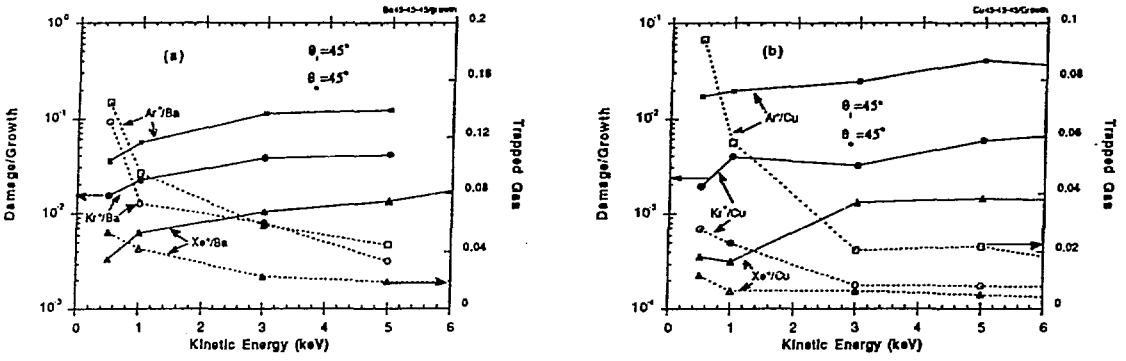

Figure 7. Normalized damage/growth and trapped gas curves, related to the synthesis of YBCO films by ion beam sputtering of elemental targets. The calculations are for Ar^+, Kr^+, and Xe^+ ions impacting on Ba (a) and Cu (b) at 45°, as a function of the kinetic energy of the primary ion.

Pulsed Ion Beam Surface Analysis

CAPABILITIES

In the preceding section, several examples of thin film applications were presented, illustrating the need for in-situ characterization of film properties in terms of average composition, lateral distribution of elements at the surface, lattice damage, impurity concentration, pinhole and island formation, and interatomic bond lengths and angles. The range of information obtainable by Direct Recoil Spectroscopy (DRS) and Ion Scattering Spectroscopy (ISS) probably exceeds that obtainable by any other surface analytical technique. Ion Scattering Spectrometry was demonstrated to be a useful means of thin film analysis by Smith in 1971 and by McKinney and Frankenthal in 1973 [Smith 1971,McKinney 1973]. The latter study used ISS as a means of characterizing 20-30 Å thick passivation layers on Fe-Cr alloys. However, ISS has not been widely used for *in-situ* thin film characterization for a number of reasons: Early ISS instruments required a very high ion beam dose, sometimes exceeding the number of atoms at the surface of the film being analyzed in order to produce usable spectra. Data acquisition times could be longer than the film deposition time. Because of the extreme surface sensitivity of the ISS technique, it is commonly perceived as suitable only for use in ultra-high vacuum and therefore incompatible with many thin film deposition methods. Additionally, most ISS analyzers including even currently marketed commercial instruments are geometrically incompatible with most deposition processes. Modern Time-of-Flight ISS instruments are either not in fact subject to most of these limitations, or can be modified to correct these difficulties. However, ToF instruments are still relatively rare, existing only as custom-built units in a few laboratories.

The method of ion beam surface analysis consists of directing an ion beam of mass M_1, kinetic energy E_o at the surface, consisting of atoms with mass M_2, and detecting either the backscattered primary particles at energy E_1 (ISS), or the direct recoil-sputtered surface atoms (DRS) with energy E_2. For primary ions in the approximate range 1-100 keV, the primary ion-target atom collisions are adequately described by two-body elastic collision dynamics. The kinetic E_1 energy of the scattered primary is then given by

$$\frac{E_1}{E_o} = (1+\alpha)^{-2} [\cos\theta_1 \pm (\alpha^2 - \sin^2\theta_1)^{1/2}]^2 \quad (1)$$

provided $M_2 > M_1$. The kinetic energy E_2 of the recoil-sputtered surface atom is

$$\frac{E_2}{E_o} = 4\alpha (1+\alpha)^{-2} \cos^2\theta_2 \quad (2)$$

where $\alpha = M_2/M_1$ and θ_1 and θ_2 are the scattering and recoil angles respectively. In addition to the single collision events represented by eqs. 1 and 2, more complicated multiple collision events sometimes give rise to relatively sharp peaks as well. These often occur at energies for which no single scattering event is possible and can usually be identified.

In order to monitor thin film deposition, it is necessary to obtain data over periods of time which are short compared with the time required for the thin film deposition process, using ion beam doses which result in negligible sputtering or other modification of the surface being studied. Since there are roughly 10^{15} atoms/cm^2 at the surface of a typical solid, a non-damaging dose may be taken as approximately 10^{13} ions/cm^2. The kinetic energies of the scattered primary and direct recoil atoms are typically measured either by using an electrostatic energy analyzer (ESA) [Smith 1967, 1971] with a continuous beam, or by pulsing the beam and measuring the time required for the scattered/sputtered particles to reach the detector after the ion beam strikes the sample [Buck 1979, Marchut 1984]. The ESA detects only ions, which typically constitute between 0.1 and 10% of the total flux leaving the sample. Moreover, at any given time, the ESA is set to transmit only a very narrow range of kinetic energies, and the spectrum is obtained by scanning this energy window.

The ToF-ISS method consists of directing a pulsed beam of energetic ions onto the surface and measuring the time at which the scattered primary particles, most of which are scattered as neutral atoms, arrive at the detector. By placing the detector either in line-of-sight with the sample, or placing the detector off-axis and applying a large bias voltage, either the scattered neutrals or ions may be selectively detected. If the scattered neutrals are detected, the method has a depth sensitivity of 3-5 atomic layers. However, since the neutralization probability for a noble gas ion penetrating more than one monolayer into the solid is nearly unity, the detection of the scattered ion species provides a sensitivity only to the uppermost atomic layer of the solid [Smith 1967, 1971, Goff 1972, Buck 1979]. This surface specificity is unique among surface analytical techniques. The ToF scheme, which independently detects backscattered ions and neutrals with kinetic energies corresponding to all M_2 values simultaneously, gains 3-4 orders of magnitude in terms of the reduction in data acquisition time and ion beam dose necessary to obtain data. Low beam dose and rapid data acquisition are key requirements for real-time, low damage *in situ* analysis of thin film growth.

The most obvious aspect of thin film analysis is to determine surface composition. A ToF-ISS spectrum obtained for 10 keV Ne^+ incident on stainless steel 304 is shown in Fig. 8.

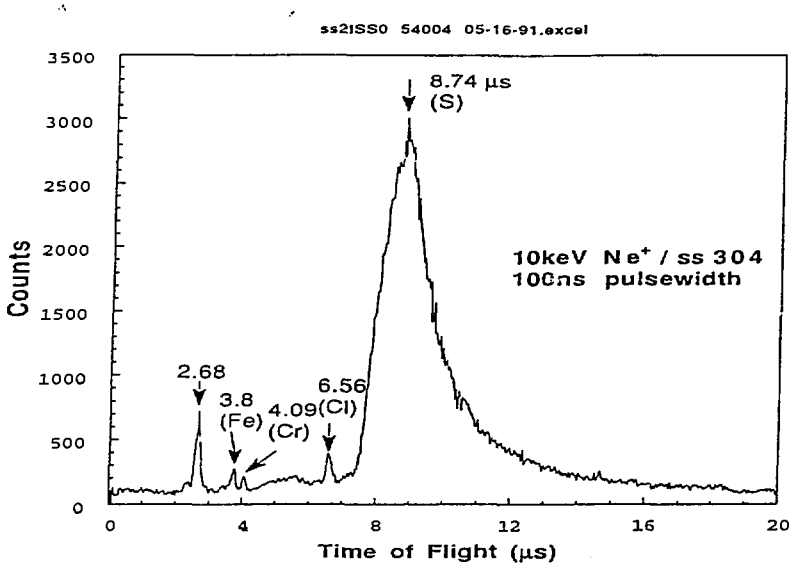

Fig. 8. Time-of-flight ion scattering spectrum of 304 stainless steel, taken with a 10 keV Ne^+ ion beam using a pulse length of 100 ns

In this figure, both scattered ions and neutrals were detected, using the ToF-ISS analyzer under development at Argonne National Laboratory. The largest peaks are seen for segregated S and Cl, which is presumably present as a surface contaminant. Fe and Cr were detected, but at much lower intensity. The unidentified peak at 2.68 µs occurs at a time which is actually less than the electronic delays in the data acquisition system and appears to correspond to a double scattering event resulting in the ejection of a relatively low mass surface hydrocarbon. Auger spectroscopy obtains its signal from a somewhat greater depth than ISS and may provide different elemental abundances. An Auger spectrum of this sample reveals relatively small amounts of S and Cl, large O and Fe peaks, a small amount of Ni and no Cr.

By varying the angle of incidence of the primary beam so that atoms designated as "B" in Fig. 9 in the second atomic layer are "shadowed" by "A" atoms in the first layer, it is possible to determine the distance and bond angle between atoms in the first few atomic layers [Brongersma 1973, Heiland 1977, Niehus 1980, Aono 1981, 1982, 1984, 1985, Marchut 1984, Taglauer 1985, Niehus 1986, 1987, Katayama 1988]. As the ion beam angle of incidence is varied, the shadowed atom may be initially totally obscured as shown in Fig. 9a, later appear at the edge of the shadow cone as shown in Fig. 9b, and eventually be totally unobstructed as shown in Fig. 9c. There is a concentration of scattered ion trajectories along the surface of the shadow cone as shown in Fig. 9b. Consequently, there is a certain angle, known as the critical angle (ψ_c), when the edge of the shadow cone starts to intercept atom B, and there is an abrupt increase in intensity corresponding to scattering from atom B. The sharpness of this increase is a measure of the mean vibrational energy of the surface atoms [Souda 1983, Niehus 1988, van de Riet 1990, Dürr 1990].

An example of the shadowing phenomenon is shown in Fig. 10 for a monolayer of Au adsorbed on Si (111) [Katayama 1988]. Since the gold is in the uppermost atomic layer, the signal intensity for backscattered primary ions is almost independent of the beam angle of incidence. It can therefore be immediately determined that the Au film is not more than one monolayer thick. For certain angles of incidence, the Si atoms are shadowed by the adsorbed Au layer, resulting in oscillations in the Si scattering intensity as a function of the angle of incidence. Similar studies on the TiC (111)-1x1 surface have shown that the C atoms are located 0.87± 0.08 Å below the surface and 1.97±0.05 Å from the nearest Ti atom, at an angle 26±1° relative to the plane of the surface [Aono 1981].

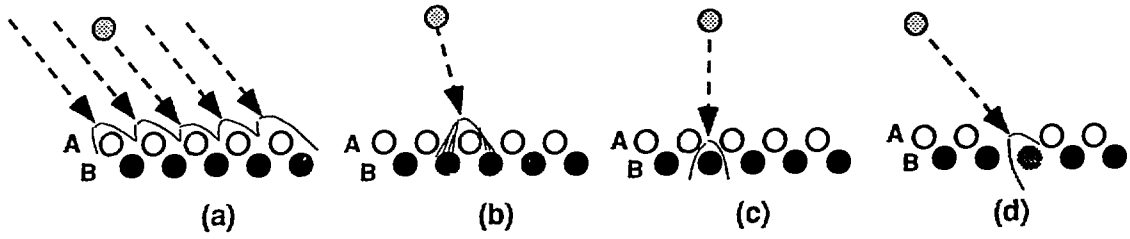

Fig. 9. Illustration of the shadowing phenomenon. (a) Atom B (black) is completely inside the shadow cone of atom A (white) and does not give rise to an ISS signal. (b) Atom B is on the edge of the shadow cone of atom A and is receiving an enhanced primary ion flux. (c) Atom B is completely outside the shadow cone of atom A. (d) All the B atoms except for one (grey) are inside the shadow cone of atom A. A missing surface atom A allows the grey atom B to be exposed to the incident primary ion flux.

If there is a surface defect as indicated in Fig. 9d in which one of the A atoms is missing, then some B atoms will be visible for angles of incidence in which the B atoms would all be in the shadow cone of the A atoms if there were no lattice defects. Consequently, there would be a bump in a plot of the peak intensity corresponding to element B as a function of angle of incidence. An example is shown in Fig. 11 for TiC (001). In this case, a carbon vacancy permits the detection of Ti atoms below the critical angle, giving rise to the structure indicated by the shaded area of Fig. 11.

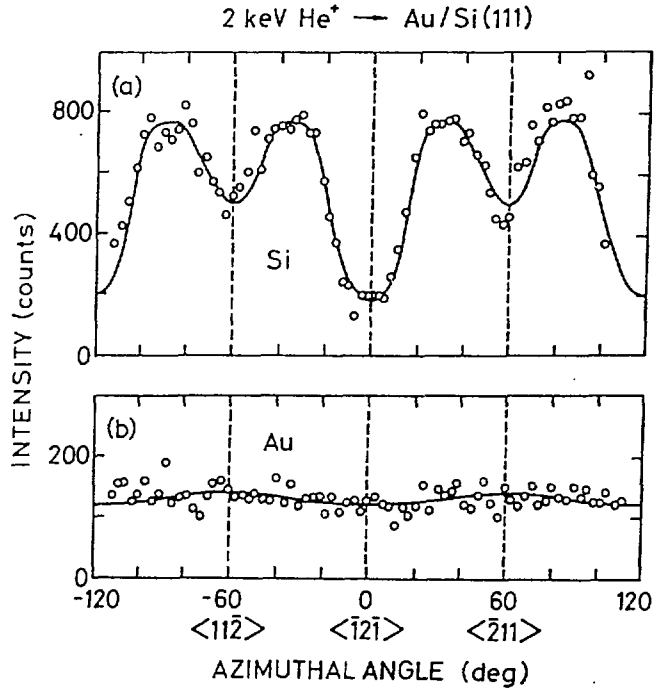

Fig. 10. Au/Si Angular variation of the Au and Si ISS signal intensity for an Au monolayer adsorbed on Si (111) (after Katayama 1988).

By mapping the intensity of specific peaks as a function of both azimuthal and polar angles, it is possible [Niehus 1991] to construct an ion beam crystallograph, showing a psuedo-three dimensional image of the atoms in the first few atomic layers. As shown in Fig. 12, such features as the atomic alignment and locations of open channels in specific crystallographic directions are clearly seen.

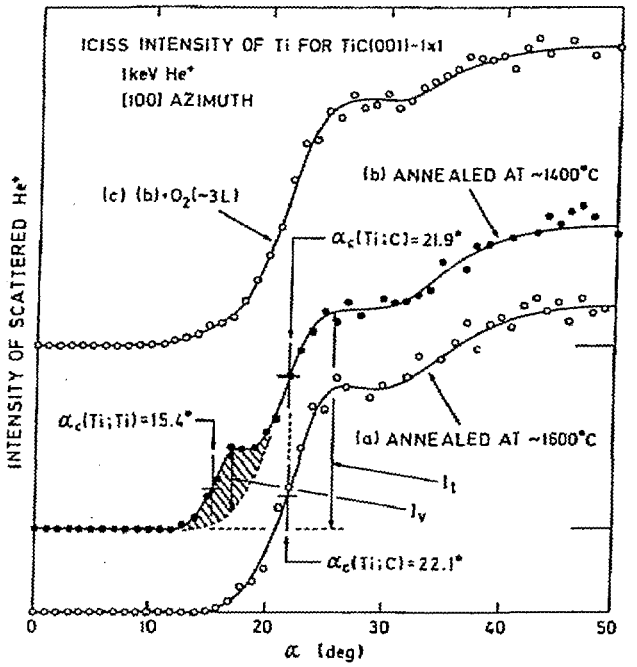

Fig. 11. Angular variation of the Ti ISS signal for a TiC surface (a) annealed and (b) with missing C atom defects (After Aono 1984).

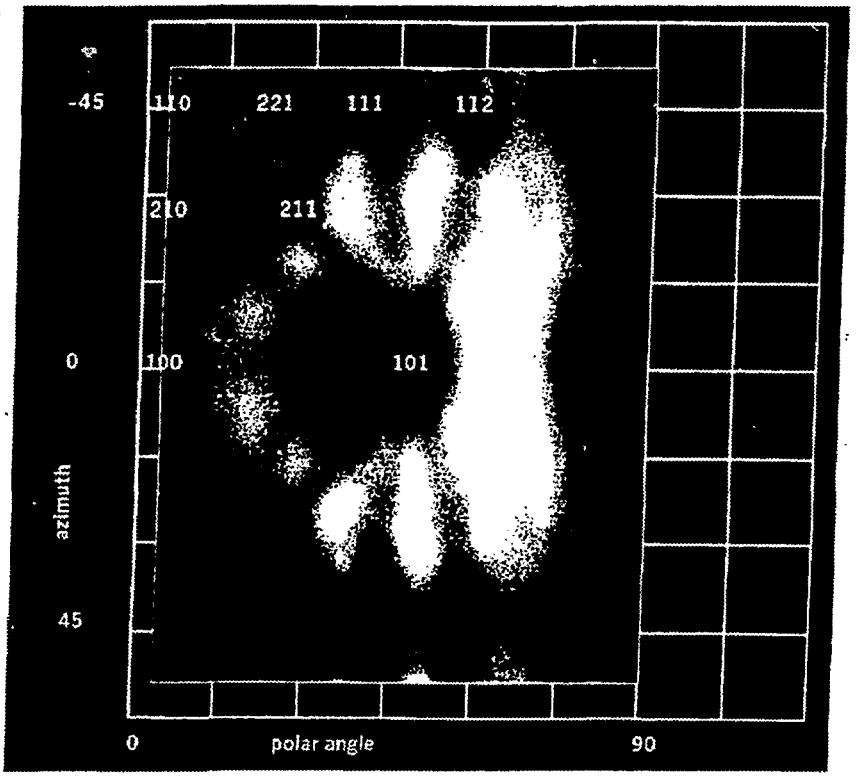

Fig. 12. Ion beam crystallograph for As/Si (001) - (1 x 2) produced by monitoring the Si ISS signal intensity as the polar and azimuthal angles were scanned. (After Niehus 1991)

By placing a detector in the forward scattering direction, surface atoms ejected by direct recoil sputtering are seen in addition to the scattered primary beam. Detection of these recoil-sputtered atoms constitutes the basis of the closely related Direct Recoil Spectroscopy (DRS) analysis technique. ISS provides no signal for ions lighter than the probe beam, but DRS is one of the few surface analytical techniques which is sensitive to helium and hydrogen, and is able to distinguish between H and D at levels down to about 1% [Schmidt 1990].

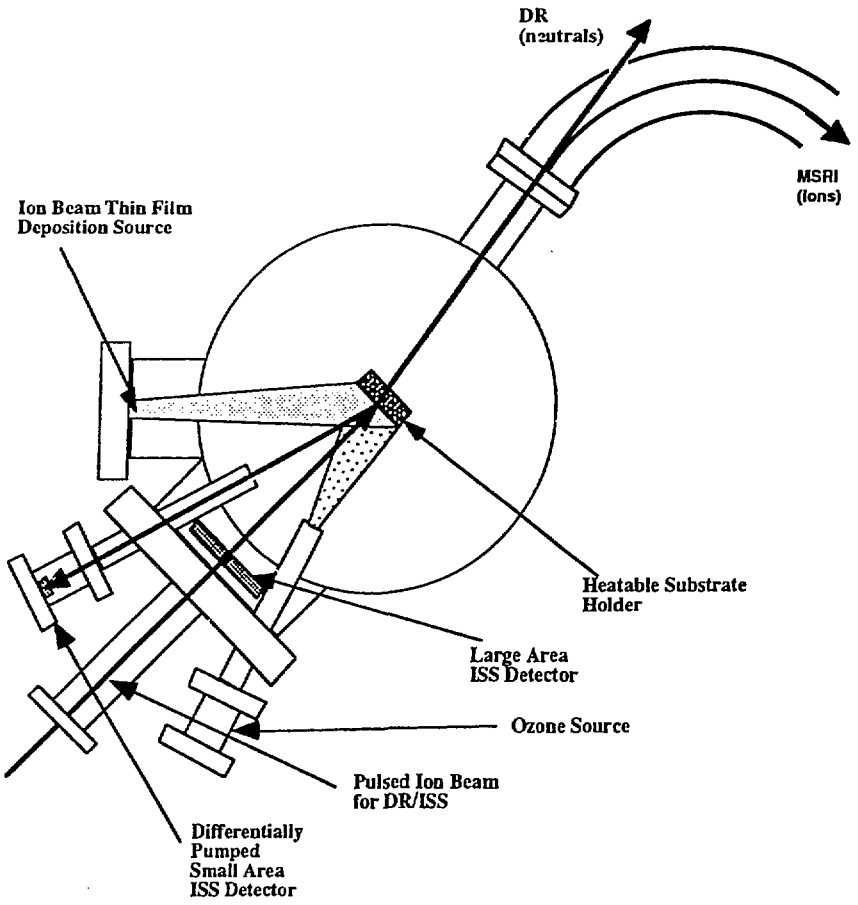

Fig. 13 Differentially pumped pulsed ion beam analysis/ion beam thin film deposition chamber, showing small and large detectors for ISS, DRS and MSRI.

Because of the long source-detector distances associated with the ToF detection scheme, the analysis method does not interfere with the equipment required for the thin film deposition process. It has been demonstrated [Katayama 1988, Aono 1989] that Time-of-Flight Ion Scattering Spectroscopy (ToF-ISS) can be used as an *in situ* monitor of thin film surface composition for low-pressure deposition processes such as MBE. However, the scattering mean free path of low keV ions is much longer than that of sub-keV electrons, and DRS and ISS are therefore much more tolerant of high background pressures than most other surface analytical methods. It has been demonstrated at higher energies, that accelerator-based ion beam analysis is possible at atmospheric pressure [Doyle 1987]. Although DRS and ISS are much more surface-specific than other surface analysis techniques, they are also much more tolerant of high background pressures. It is also possible to provide differential pumping of the incoming and outgoing ion beam paths to

extend the pressure limits of the ToF ion beam techniques even further, as shown in Fig. 13. This capability has been demonstrated for DRS of diamond-like films during growth by Low Pressure Chemical Vapor Deposition (LPCVD) at pressures up to 1 Torr, and hydrogen adsorption has been measured on (100) diamond at ambient pressures up to 330 mTorr with very little loss of resolution [Schmidt 1990] as shown in Fig. 14. This represents a 6-8 order of magnitude increase in the permissible operating pressure compared with other surface analytical methods.

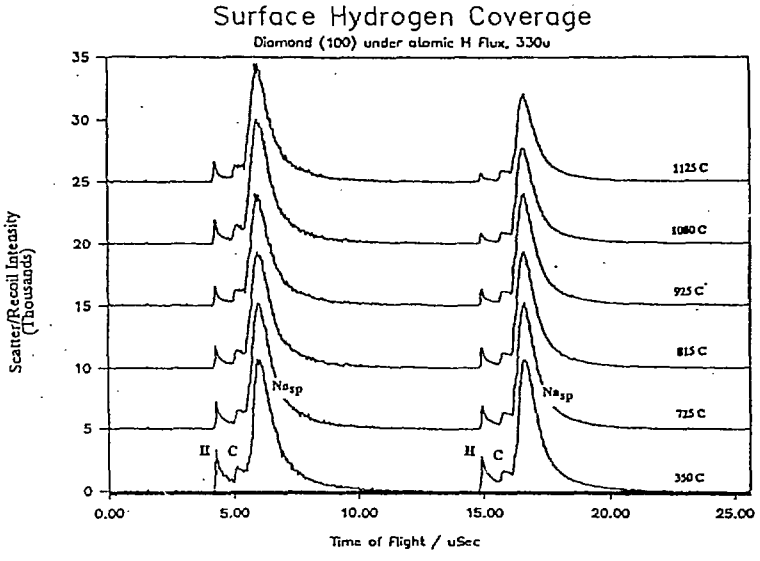

Fig. 14. Direct Recoil spectrum of a diamond (100) film exposed to a flux of atomic hydrogen in an ambient pressure of 330 μTorr. Data was taken using a 6 keV Na^+ beam.

A technique related to ISS and DRS, Mass Spectroscopy of Recoiled Ions (MSRI), has been developed by Ionwerks, Inc. As shown in Fig. 13, the neutral direct recoils impinge on an electron multiplier which is in line of sight with the target. The output of this detector constitutes the DRS signal. The recoiled ions however, are deflected into a ToF Poschenrieder-type mass analyzer. The instrumentation is very similar to that of ToF Secondary Ion Mass Spectrometry (SIMS) except that the positioning of the analyzer is such that the direct recoils are preferentially detected with respect to the cascade-ejected secondary ions. The DR ions have much higher kinetic energy than the SIMS ions and are therefore able to penetrate a region of much higher ambient pressure without significant scattering. Consequently, the pressure limit of MSRI is expected to be similar to that of ISS and DRS. The ultimate sensitivity and mass resolution appear to be similar to that of ToF-SIMS except that as a result of the higher kinetic energy associated with the DR process, there is less neutralization of the ejected ions in the near-surface region, and consequently a reduction in the undesirable matrix effect which makes SIMS very difficult to quantify. For elements such as boron, in which the SIMS secondary ion fraction is very low, MSRI may be more sensitive. A MSRI spectrum of a BN film, obtained in 20 seconds, is shown in Fig. 15. The demonstrated resolution is significantly better than most quadrupole-based SIMS instruments. A recent design modification has improved the MSRI signal to noise ratio and resolution even further, yielding a dynamic range of 10^9 (sensitivity < 1 ppb) and mass resolution of 400 at mass 238. The time necessary to acquire a spectrum comparable to Fig. 15 is now well under one second. It is anticipated that MSRI will be extremely valuable for real-time quantitation of majority elements, dopants, minority impurities, and film-substrate interdiffusion during thin film

deposition, perhaps achieving new detection limits for trace elements where SIMS has limited sensitivity (e.g., N in GaAs). Because of the absence of the SIMS matrix effect, the results, can be made quantitative to within 5%, compared to a typical value of ±50% for SIMS .

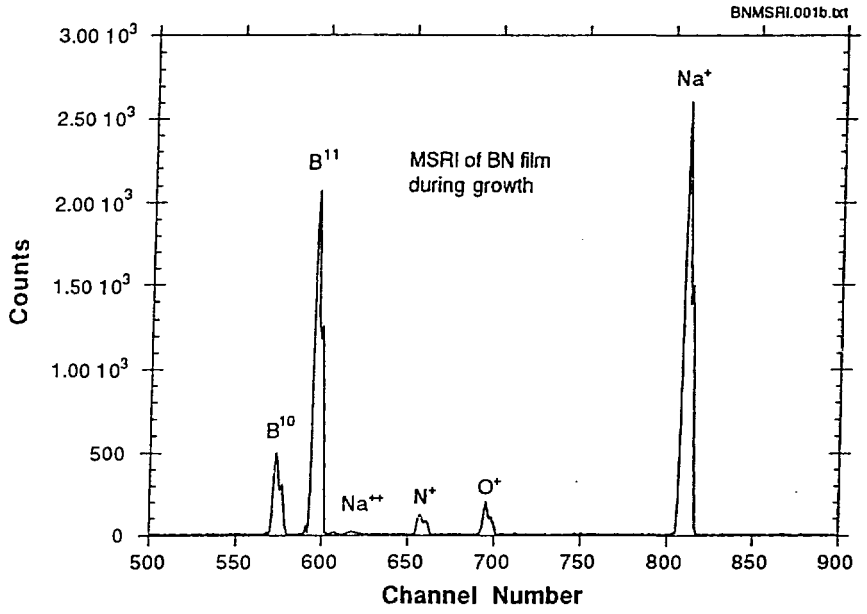

Fig. 15 MSRI spectrum of a BN film during growth at 10^{-4} Torr.

INSTRUMENTATION

A Time-of-Flight Direct Recoil and Ion Scattering Spectrometer (ToF-DR/ISS) system is currently under development at Argonne. This system has been used to demonstrate extremely low dose surface analysis, very high data acquisition rate, and considerably greater flexibility of operation than previous designs. A thin film multi-target ion beam growth chamber [Krauss 1990] has been added as an appendage to the analysis chamber, permitting real-time monitoring of the growth of multicomponent metal and metal oxide thin films and layered structures.

Pulse Formation

The beam line is shown in Fig. 16. It consists of a telefocus ion source injecting a 5-12 keV mass analyzed ion beam into a transfer section containing two deflection regions separated by a drift space. A dc beam current of 1-2 μA may be directed through the beam line onto the sample at 10 keV. The apertures A1-A4 may be adjusted *in situ*, selecting from 6 sizes ranging from 250 μm to 4 mm in diameter. The current reaching the sample is proportional to the area of the selected aperture size as shown in Fig. 17, indicating that the beam is essentially paraxial. For pulsed operation, the deflection voltages are added to the dc offsets which are adjusted to provide maximum beam current when the apertures are slightly out of alignment in order to eliminate energetic charge-exchange neutrals from the beam. The voltage pulses which are applied to the deflection plates are of fixed width, with very short rise time. The time between the leading edge of

the first pulse and the falling edge of the second pulse determines the temporal length of the ion beam pulse. The data acquisition software determines the timing to provide the ion beam pulse length specified by the operator. The pulse length can be adjusted from ~10 ns to 1 μs. It is therefore possible to adjust the pulse length to suit the needs of the measurement.

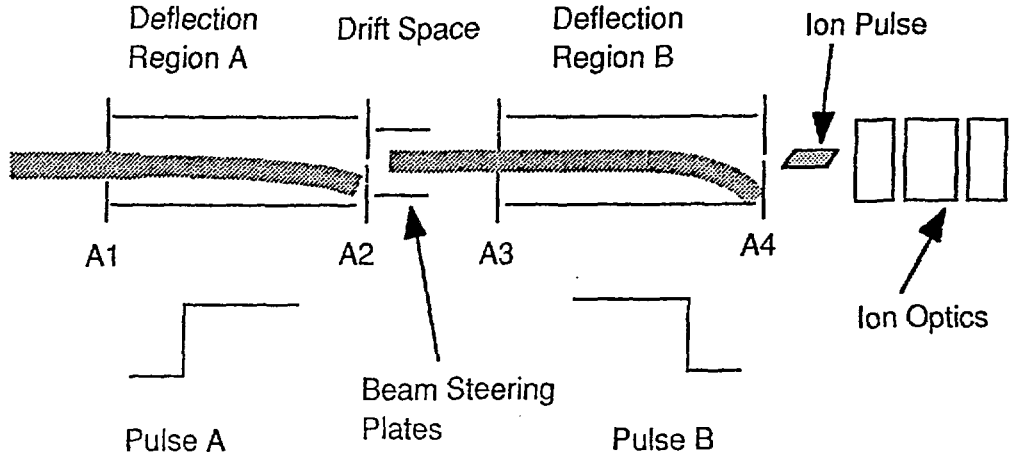

Fig. 16 Schematic diagram of the Dual Pulsed Beam Line with microfocus capability.

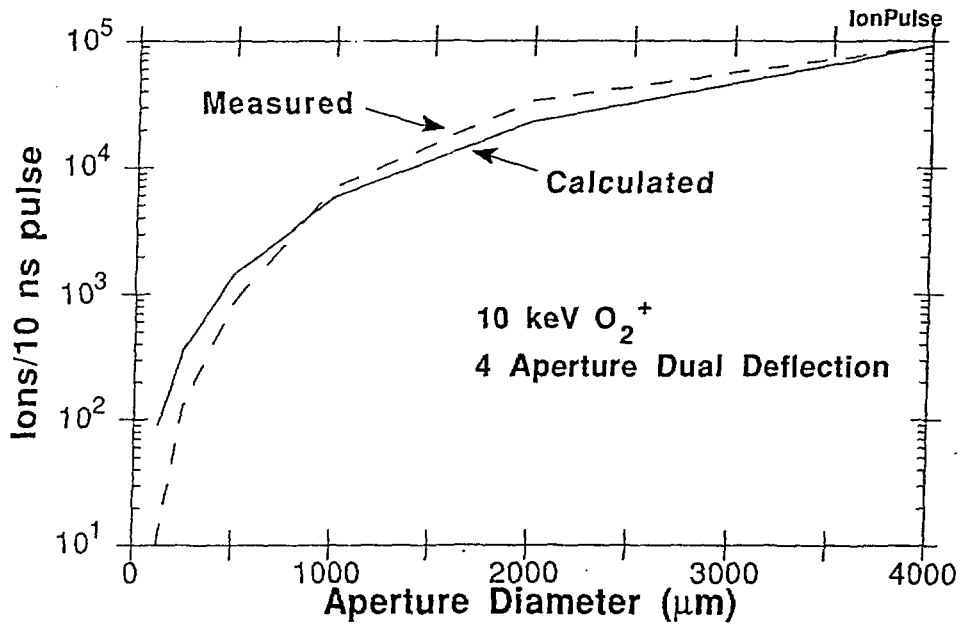

Fig. 17. Plot of the calculated and measured beam current incident on a sample located 30 cm from the exit aperture of the beam line shown in Fig. 16 as a function of aperture size.

A short ion beam pulse provides good mass resolution and exhibits a distinctly asymmetric peak, as shown in Fig. 18, for detection of both ion and neutral Ar scattered into a small area detector from a sample of 304 stainless steel. Auger analysis, which has a sampling depth of 10-15

Å, shows a surface consisting largely of Fe, with almost no Cr visible. The large Cr peak in Fig. 18 results from the fact that ISS is primarily sensitive to the composition of the first atomic layer, which is strongly enriched in Cr. The long flight time tail of the Cr peak results from scattering of the primary beam by atoms in the second, third, and fourth atomic layers. A similar asymmetry has been observed in DRS data, and the shape has been calculated by Eckstein [Eckstein 1987]. In principle, the shape of the long flight time tails can be deconvoluted to provide information on the depth distribution of each atomic species in the first few atomic layers.

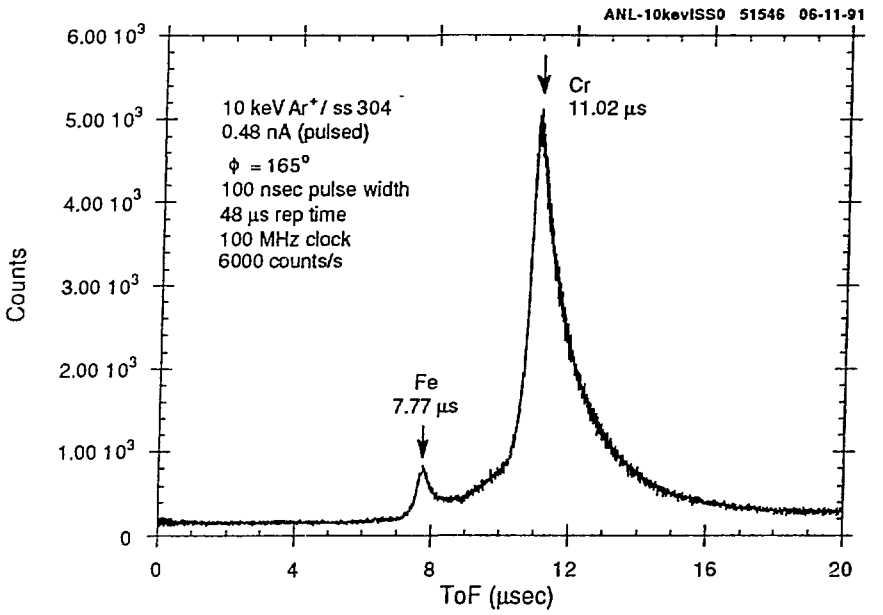

Fig. 18 ToF-ISS spectrum of stainless steel taken with a 1-cm diameter detector in the ANL DR/ISS system.

A long ion beam pulse results in decreased mass resolution, as shown in Fig. 19, but provides significantly increased count rate. The total ion dose used for the spectra of Figs. 18 and 5.7 was ~10^{12} ions. However, the mass resolution of Fig. 18 is more than adequate for elemental identification and it is possible to obtain useful data with much lower ion doses (~10^{10} ions), as shown in Fig. 20.

It is instructive to compare the spectra obtained with the ANL ToF-ISS system with data on a similar sample (Fig. 21), which was obtained with the 127 degree electrostatic ISS analyzer used by McKinney and Frankenthal [McKinney 1973]. Both the signal/noise ratio and resolution are much inferior to the data shown in Figs. 18 and 19. In addition, the ion beam dose is on the order of 10^{15} ions/cm^2, for a mass scan covering the range 50-58 amu. Such a diagnostic is of course useless for continuous *in situ* monitoring of thin film growth since the film would be sputtered by the analysis beam as rapidly as it is deposited. Newer electrostatic analyzers give an improved signal/noise ratio but intrude severely into the deposition region, making them useless as an *in situ* monitor of thin film deposition.

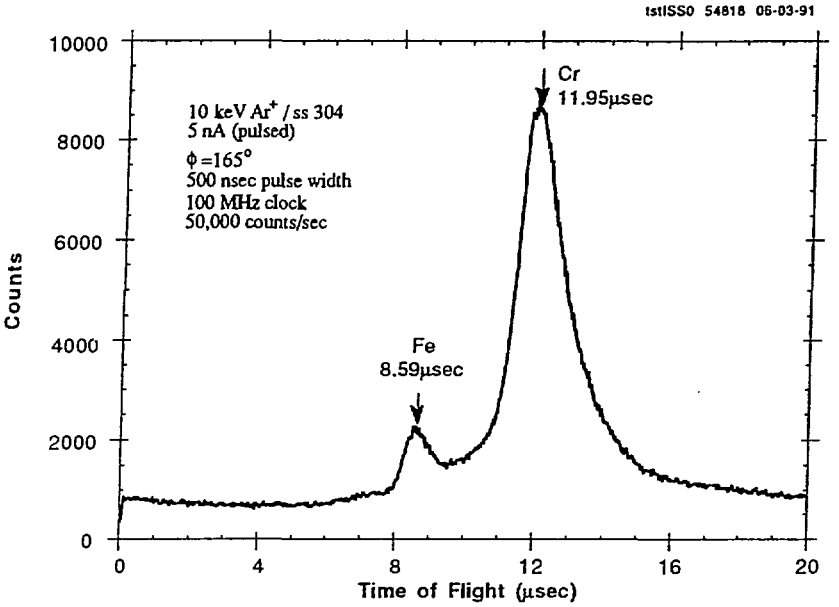

Fig. 19 ToF-ISS spectrum of stainless steel taken with a 1-cm diameter detector in the ANL DR/ISS system using a 500 nsec pulse width.

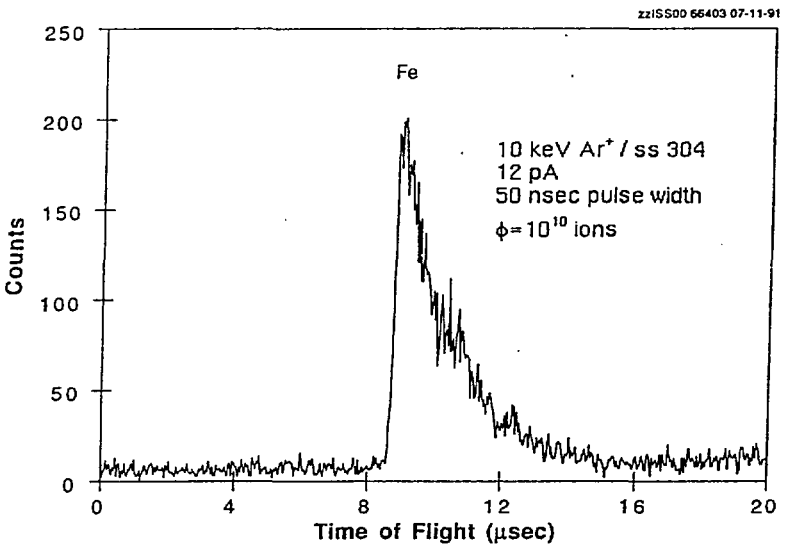

Fig. 20 ToF-ISS spectrum of stainless steel taken with a 1-cm diameter detector in the ANL DR/ISS system using a beam dose of 10^{10} ions.

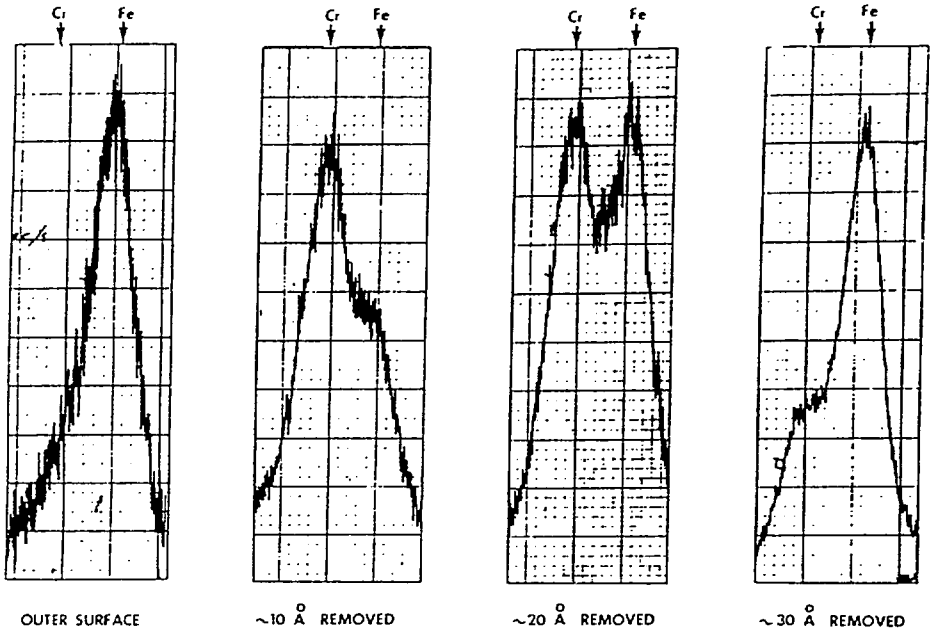

Fig. 21 ISS spectrum of stainless steel taken with 127° electrostatic analyzer (McKinney 1973)

The spectra shown in Figs. 18-20 were taken using a small (1 cm diameter) spiraltron detector. As described below, the installation of a large area channel plate detector will reduce the required dose an additional two orders of magnitude. At that point, the ion dose will be competitive with the much more complex and expensive laser resonance ionization technique, which currently holds the record as the most sensitive surface analytical method known.

Beam Characteristics

The transmitted ion pulse forms a footprint on the sample surface consisting of a stationary "hotspot" along with a much less intense "corona" arising from the tail of the chopped ion beam, which moves as the beam is pulsed. Details of the pulse characteristics will be presented elsewhere [Krauss 1992a]. For long ion beam pulses and short rise time deflection voltages, the current contained in the corona becomes negligible in comparison with the stationary hotspot. The hotspot can be focused and rastered across the surface, thereby functioning as a microprobe. Because of the high count rate associated with the use of long ion beam pulses and the large area detector (described below), reasonably short data acquisition times of scanned images are possible, limited primarily by the speed with which the computer is able to read the data from the histogram memory and assemble the images. Preliminary results indicate that good imaging signal/noise should be obtained with a dose of 10^7-10^8 ions per pixel. We define the term "static" ion beam dose as a dose which is small enough to cause negligible damage, corresponding to a maximum of approximately 1% of the atoms in the surface area exposed to the beam, or typically about 10^{13} ions/cm^2. The smallest spot which may be resolved by the Argonne DR/ISS system using the large area detector, while not exceeding this dose is ~5 μm in diameter. Using a light probe ion such as He which results in both a reduced damage level and a higher fraction of backscattered primary ions, the diameter of the minimum area which may be resolved while keeping the damage below the 1% level is approximately 1 μm. By comparison, the corresponding beam diameter for the 127 degree analyzer used by McKinney and Frankenthal [McKinney 1973] is 10 cm.

Detectors

The system has five detectors, of which four are differentially pumped, permitting analysis of samples which are at ambient pressures approaching one Torr. The differentially pumped detectors are spiraltron electron multipliers with a 1 cm. diameter collection cone, located approximately 50 cm from the sample. They are geometrically arranged so that in both the backscattering and direct recoil directions, there are two detectors. One detector is off-axis and detects the ion signal, while the other is in line of sight with the sample and detects energetic neutrals. The fifth detector is a 4 cm. diameter channel plate with a segmented anode collector consisting of 8 concentric rings, each connected to a separate preamplifier and discriminator, located 25 cm from the sample. Each segment corresponds to scattering into a well-defined polar angle, and therefore a peak in the ToF spectrum corresponds to a well-defined surface species with mass M_2. The spectra collected by each segment, are stored separately in a histogram memory. The time-of-flight axis is converted to an M_2 scale by the data acquisition software and the spectra from the various detector segments are then added to produce a composite spectrum which has the same mass resolution as that of the differentially-pumped small area detectors but 64x higher count rate (or equivalently, 64x lower beam dose for the same signal/noise ratio). The high data acquisition rate obtainable with this detector, coupled with the high count rate provided by the use of relatively long ion pulses and the stable beam position resulting from the dual beam chopping scheme will permit the development of a scanning ISS microprobe, and is expected to reduce the time required for a complete polar-azimuthal angular scan from approximately 10 hours to 10 minutes.

Data Acquisition

The ability to use long beam pulses, along with a high beam current and the extremely high signal collection efficiency afforded by the large area detector combine to produce an exceptionally high count rate for a ToF instrument. Preliminary measurements using the small area detector produce count rates of 5-50 kHz. Based on this result, the estimated count rate using the large area detector exceeds 3 MHz. Software histogramming at this rate is not feasible. We have developed a system in which the data acquisition computer pre-sets the ion beam pulse width and pulse repetition rate, and reserves up to 16 regions of a CAMAC histogram memory for various purposes. The small area detectors can each utilize up to 8 regions, corresponding to 8 detected particles per ion beam pulse. The large area detector uses 8 regions, one for each segment of the divided anode. Once data acquisition has been started, a quartz controlled clock on the data acquisition card controls the pulse repetition rate without further software intervention, and the data is assembled into the requisite number of histograms under hardware control. Consequently, the computer is able control the deposition process and simultaneously assemble composite spectra obtained by the large area detector, display the data, control beam position and build images of the elemental distributions on the surface without disrupting the data acquisition process. Details of the data acquisition hardware will be presented elsewhere. [Krauss 1992b]

Summary

Ion beam-surface interactions produce many effects in thin film deposition which are similar to those encountered in plasma deposition processes. However, because of the lower pressures and higher directionality associated with the ion beam process, it is easier to avoid some sources of film contamination and to provide better control of ion energies and fluxes. Additional effects occur in the ion beam process because of the relatively small degree of thermalization resulting from gas phase collisions with both the ion beam and atoms sputtered from the target. These effects may be either beneficial or detrimental to the film properties, depending on the material and deposition conditions. Ion beam deposition is particularly suited to the deposition of multi-component films and layered structures, and can in principle be extended to a complete device fabrication process.

However, complex phenomena occurr in the deposition of many materials of high technical interest which make it desirable to monitor the film growth at the monolayer level. It is possible to make use of ion-surface interactions to provide a full suite of surface analytical capabilities in one instrument, and this data may be obtained at ambient pressures which are far too high for conventional surface analysis techniques. Such an instrument is under development, and its current performance characteristics and anticipated capabilities are described.

Acknowledgement

This work has been supported in part by the U. S. Department of Energy, Office of Basic Energy Sciences under contract W-31-109-ENG-38 and by the State of Illinois Dept. of Commerce and Community Affairs.

References

A. R. Krauss, O. Auciello, A. I. Kingon, M. S. Ameen, Y. L. Liu, T. Barr, T. M. Graettinger, S. H. Rou, C. S. Soble and D. M. Gruen, Applied Surface Science **46**, 67 (1990)

A. I. Kingon, O. Auciello, M. S. Ameen, C. N. Soble, T. M. Graettinger, S. H. Rou, and A. R. Krauss, Proc. Symp. on Thin and Thick Films, Amer. Ceramic Society, B. V. Hiremath, ed., Acers, Westerville, OH (1991) p. 147

M. Hawley, I. D. Raistrick, J. G. Beery, and R. J. Houlton, Science 251, 279 (1991)

C. Weissmantel, G. Reisse, H. J. Erler, F. Henny, K. Bewilogua, U. Ebersbach, and C. Schurer, Thin Solid Films **3**, 315 (1979)

C. Weissmantel, K. Bewilogua, K. Breauer, D. Dietrich, U. Ebersbach, H. J. Erler, B. Rau and G. Reisse, Thin Solid Films **96**, 31 (1982)

J. M. E. Harper, J. J. Cuomo, and H. R. Kaufman in Ion Bombardment of Surfaces: Fundamentals and Applications (O. Auciello and R. Kelly eds., Elsevier, Amsterdam 1984)

C. Weissmantel, J. Vac. Sci. Technol. **18**, 179 (1981)

J. Linnros, B. Svennson and G. Holmen, Phys. Rev. **B30**, 3629 (1984)

J. Linnros, G. Holmen and B. Svennson, Phys. Rev. **B32**, 2770 (1985)

J. S. Williams, R. G. Elliman, W. L. Brown and T. E. Seidel, Phys. Rev. Lett. **55**, 1482 (1985)

H. A. Atwater, H. I. Smith and C. V. Thompson, in Beam-Solid Interactions and Phase Transformations, H. Kurz, G. L. Olson and J. M. Poate eds. (Materials Research Society, Pittsburgh PA 1986), pp. 337-342

P. Wang, D. A. Thompson and W. W. Smeltzer, Nucl. Instr. Meth. **B7/8**, 97 (1986) and B16, 288 (1988)

J. C. Liu and J. W. Mayer Nucl. Instr. Meth. Phys. Res. **B19/20**, 538 (1987a)

J. C. Liu, M. Nastasi and J. W. Mayer , J. Appl. Phys. **62**, 423 (1987b)

H. A. Atwater, Carl V. Thompson and Henry I. Smith, Phys. Rev. Let. **60**. 112 (1988)

J. Li, J. C. Liu and J. W. Mayer, Nucl. Instrum. Meth. **B36**, 306 (1989)

D. E. Alexander and G. S. Was, Mat. Res. Soc. Symp. Proc. **202**, 205 (1991)

T. C. Huang, G. Lin, F. Parmigiani and E. Kay, J. VAc. Sci. Technol. **A3**, 2161 (1985)

P. Ziemann and E. Kay, J. Vac. Sci. Technol. **A1**, 512 (1983)

G. E. Thomas, L. J. Beckers, J. J. Vrakking and B. R. de Koning, J. Cryst. Growth **56**, 257 (1982)

P. C. Zalm and L. J. Beckers, Appl. Phys. Lett. **41**, 167 (1982)

T. Takagi, J. Vac. Sci. Technol. **A2**, 382 (1984)

F. J. A. den Broeder, D. Kuiper and H. J. G. Draaisma, IEEE Trans Mag. **23**, 3696 (1987)

M. S. Ameen, O. Auciello, A. I. Kingon, A. R. Krauss and M. A. Ray, AIP Conf. Proc. **200** (High Tc Supercond. Thin Film Process, Charact. Apl) 79, 1990

A. R. Krauss and O. Auciello, Mat. Res. Soc. Symp. Proc. 1992, in press

W. Eckstein, J. Nuclear Fusion Suppl. **1**, 17 (1991)

P. F. Carcia and S. I. Shah, Appl. Phys. Lett. **56**, 2345 (1990)].

T. Miyazawa, S. Misawa, S. Yoshida and S. Gonda, Japan J. Appl. Phys. **55**, 188 (1984)

J. C. Angus, P. Koidl, and S. Domitz, Carbon Thin Films in Plasma Deposition of Thin Films, J. Mort and F. Jansen eds., CRC Press, Boca Raton FL, (1986)

W. Moller, Diamond and Diamond-Like Films and Coatings, R. Clausing, ed., Plenum Press, New York, 1991, p. 229

K. G. Tschersich, J. Nucl. Mater. 162, 887 (1989)

L. Holland and S. M. Ojba, Thin Solid Films **48**, 21 (1978)

S. Berg and L. P. Anderson, **58**, 117 (1979)

S. Kasi, H. Kang and J. W. Rabalais, Phys. Rev. Lett. **59**, 75 (1987)

S. Kasi, H. Kang and J. W. Rabalais, J. Chem. Phys. **88**, 5914 (1988)

J. Kulik, Y. Lifshitz, G. D. Lempert, J. W. Rabalais and D. Marton, Proc. 50th Ann. Mtg. Electron Microscopy Soc. America, San Francisco Press, San Francisco, CA 94142-6800 (in press, 1992)

R. J. Meilunas, R. P. H. Chang, S. Liu and M. Kappes, Appl. Phys. Lett. **59**, 3461 (1991)

M. Muroi, Y. Okamura, T. Suzuki, K. Tsuda, M. Nagano and K. Mukae, Jpn. J. Appl. Phys., in press, 1992

S. M. Rossnagel and J. J. Cuomo, Amer. Inst. of Phys. Conf. Proc. "Thin Film Processing and Characterization of High Temperature Superconductors", J. M. E. Harper, R. J. Colton and L. C. Feldman eds. No. **165**, 106 (1988)

M. S. Ameen , T. M. Graettinger, O. Auciello, S. H. Rou, A. I. Kingon and A. R. Krauss, Mat. Res. Soc. Symp. Proc. **152**, 175 (1989)

D. J. Lichtenwalner, O. Auciello, R. R. Woolcott, Jr. C. N. Soble , R. Adu/Poku, R. Chapman, S. H. Rou, J. Duarte, A. I. Kingon J.Vac. Sci. Technol. A in press (1992)

J. A. Kittl, C. W. Nieh, D. S. Lee and W. L. Johnson, Met. Lett. 9, 336 (1990a); also Appl. Phys. Lett. 56, 2468 (1990b)

J. A. Kittl, W. L. Johnson, and C. W. Nieh, J. Appl. Phys. 69, 6710 (1991)

C. N. Soble, D. J. Lichtenwalner, R. R. Woolcott, O. Auciello and A. I. Kingon, in preparation

W. Eckstein and J. P. Biersack, Z. Phys. **B63**, 471 (1986)

A. R. Krauss and O. Auciello, A. R. Krauss and O. Auciello, Proceedings of the Spring Meeting of the Materials Research Society, San Francisco CA, April 27-May 1, 1992 (in press)

D. P. Smith, Surf. Sci. **25**, 171 (1971)

J.T. McKinney and R.P. Frankenthal, Proc. Annual Meeting National Association of Corrosion Engineers, March 22, 1973, Anaheim, CA.

D. P. Smith, J. Appl. Phys. **38**, 340 (1967)

D. P. Smith, Surf. Sci. **25**, 171 (1971)

L. Marchut, T. M. Buck, G. H. Wheatley and C. J. McMahon, Jr., Surf. SCi. **141,** 549 (1984)

R. Goff, J. Vac. Sci. Technol. **10**, 355 (1973)

T. M. Buck, G. H. Wheatley and L. K. Verheij, Surf. Sci. **90**, 635 (1979)

H. H. Brongersma, J. Vac. Sci. Technol. **11**, 231 (1974)

W. Heiland and E. Taglauer, Surf. Sci. **68**, 96 (1977)

H. Niehus and G. Comsa, Suirf. Sci. **93**, L147 (1980)

M. Aono, C. Oshima, S. Zaima, S. Otani and Y. Ishizawa, Japn. J. Appl. Phys. **20**, L829, 1981

M. Aono, Y. Hou, C. Oshima and Y. Ishizawa, Phys. Rev. Lett. **49**, 567 (1982)

M. Aono, Nucl. Instr. Meth. Phys. Res. **B2**, 374 (1984)

E. Taglauer, Appl. Phys. **A38**, 161 (1985)

H. Niehus and G. Comsa, Nucl. Instr. Meth. Phys. Res. **B15**, 122 (1986)

H. Niehus, J. Vac. Sci. Technol. **A5**, 751 (1987)

M. Katayama, E. Nomura, N. Kanekama, H. Soejima, and M. Aono, Nucl. Instr. Meth. Phys. Res. **B33**, 857 (1988)

M. Aono and R. Souda, Jpn. J. Appl. Phys. **24**, 1249 (1985)

R. Souda, M. Aono, C. Oshima, and Y. Ishizawa, Surf. Sci. **128**, L236 (1983)

H. Niehus, K. Mann, B. N. Eldridge, and M. L. Yu, J. Vac. Sci. Technol. **A6**, 625 (1988)

E. VAn de Riet, J. M. Fluit, and A. Niehaus, Vacuum **41**, 372 (1990)

H. Dürr, R. Schneider, and Th Fauster, Vacuum **41**, 376 (1990)

H. Niehus and R. Spitzl, Surface and Interface Analysis **17**, 287 (1991)

H. K. Schmidt, J. A. Schultz and Z. Sheng, Proc. NATO ASI, Castelvecchio, Italy, July 22-Aug. 3, 1990

M. Aono, M. Katayama, E. Nomura, T. Chasse, D. Choi and M. Kato, Nucl. Instr. Meth. **B37**, 264 (1989)

B. L.Doyle, R. T. McGrath, A. E. Pontau, Nucl. Instrum. Meth. Phys. Res. B22, 34 (1987)

A. R. Krauss, O. Auciello, A. I. Kingon, M. S. Ameen, Y. L. Liu, T. Barr, T. M.Graettinger, S. H. Rou, C. S. Soble and D. M. Gruen, Applied Surface Science **46**, 67 (1990)

W. Eckstein, Nucl. Instrum. Meth. Phys. Res. **B27**, 78 (1987); D. M. Gruen, A. R. Krauss, M. J. Pellin and C. E. Young, eds.

A. R. Krauss, M. Rangaswamy, in preparation, 1992a

A. R. Krauss, J. G. Lamich and D. M. Gruen, in preparation, 1992b